

ARTICLE

Received 8 Dec 2014 | Accepted 9 May 2015 | Published 1 Jul 2015

DOI: 10.1038/ncomms8446

OPEN

Cooper pair splitting in parallel quantum dot Josephson junctions

R.S. Deacon^{1,2}, A. Oiwa³, J. Sailer⁴, S. Baba⁴, Y. Kanai³, K. Shibata^{5,6}, K. Hirakawa^{5,6,7} & S. Tarucha^{2,4,6,8}

Devices to generate on-demand non-local spin entangled electron pairs have potential application as solid-state analogues of the entangled photon sources used in quantum optics. Recently, Andreev entanglers that use two quantum dots as filters to adiabatically split and separate the quasi-particles of Cooper pairs have shown efficient splitting through measurements of the transport charge but the spin entanglement has not been directly confirmed. Here we report measurements on parallel quantum dot Josephson junction devices allowing a Josephson current to flow due to the adiabatic splitting and recombination of the Cooper pair between the dots. The evidence for this non-local transport is confirmed through study of the non-dissipative supercurrent while tuning independently the dots with local electrical gates. As the Josephson current arises only from processes that maintain the coherence, we can confirm that a current flows from the spatially separated entangled pair.

¹Advanced Device Laboratory, RIKEN, Wako 351-0198, Japan. ²Center for Emergent Matter Science (CEMS), RIKEN, Wako 351-0198, Japan. ³The Institute of Scientific and Industrial Research, Osaka University 8-1 Mihogaoka, Ibaraki 567-0047, Japan. ⁴Department of Applied Physics, The University of Tokyo, 7-3-1 Hongo, Bunkyo-ku, Tokyo 113-8656, Japan. ⁵Institute of Industrial Science, The University of Tokyo, 4-6-1 Komaba, Meguro-ku, Tokyo 153-8505, Japan. ⁶INQIE, The University of Tokyo, 4-6-1 Komaba, Meguro-ku, Tokyo 153-8505, Japan. ⁷JST CREST, 4-1-8 Hon-cho, Kawaguchi-shi, Saitama 332-0012, Japan. ⁸QPEC, The University of Tokyo, 7-3-1 Hongo, Bunkyo-ku, Tokyo 113-8656, Japan. Correspondence and requests for materials should be addressed to R.S.D. (email: russell@riken.jp).

Since the famous Gedankenexperiment of Einstein, Podolsky and Rosen¹ and later experimental demonstration of quantum non-locality², the phenomenon of quantum entanglement has been accepted as a fundamental feature of quantum mechanics. Quantum entanglement has been identified as a useful property for application in both computation and communication³. While entanglement itself is ubiquitous, the preparation and isolation of useful entangled states such as a maximally entangled Einstein–Podolsky–Rosen (EPR) pair is non-trivial. Most headway in this area has been made in quantum optics in which the sources of EPR pairs are well established and already applied for long distance quantum communication⁴. In the solid state, an EPR source for entangled electrons is highly desirable as a circuit element for a quantum information processor allowing the production of EPR pairs to be used for the teleportation of qubit states across a chip. One attractive proposal for a solid-state EPR source utilizes a superconductor as a natural reservoir for EPR pairs, which could be extracted and separated on-demand^{5–11}. In a BCS superconductor, a Cooper pair is composed of two electrons with opposite momenta and spin singlet state paired through an attractive electron–electron interaction mediated by phonons. Intuitively, the spatial extent of the Cooper pair given by the BCS coherence length ξ_0 imposes a restriction on the possible separation between contacts into which the Cooper pair could be split. In practice, however, the probability of splitting the Cooper pair into two spatially separated leads is a function of both ξ_0 and the Fermi wavelength λ_F (refs 6,12,13). Most experimental studies to date have used nanotubes^{14,15} or nanowires^{16,17} in which the proximity effect in the sections of nanotube or wire between the quantum dots (QDs) can lead to an increased probability for splitting¹⁸. Despite the limitation on the efficiency of splitting based on the probability of separating the Cooper pair, several groups have reported indications of highly efficient splitting of Cooper pairs in QD Y-junction devices^{14–17} with recently reported efficiency approaching unity¹⁵. The strong electron–electron interaction on the QDs suppresses the tunnelling of Cooper pairs through a single dot and therefore reinforces the process of crossed Andreev reflection allowing the separation of Cooper pairs into the two metal leads. Measurements have probed the Cooper pair splitting through observation of non-local charge signals^{14–16} and correlation of the current fluctuations¹⁷. However, in these first measurements, the entangled spin state is not directly confirmed.

In this work, we study a device in which two QDs are placed in close proximity within a nanogap between two superconducting leads, a system so far only considered in a small number of theoretical studies^{19–21}. By measuring the supercurrent in this

device, we detect its enhancement when Cooper pairs from one lead are split between the two QDs and then recombined in the second lead.

Results

Device details. The device studied consists of two self-assembled InAs QDs contacted with Ti/Al (3/150 nm) source and drain electrodes, Fig. 1. In our device, each QD can be independently tuned using voltages V_{sg1} and V_{sg2} applied to local side-gates allowing control of the local energy levels ϵ_{d1} and ϵ_{d2} for QD1 and QD2, respectively. A voltage V_{bg} applied to a global backgate allows tuning of the occupation of both QDs simultaneously and allows us to probe a wider range of charge states in both QDs. If the spatial separation of the contact to the two QDs is less than the superconducting coherence length (ξ_0), we may expect crossed Andreev reflection processes where a single Cooper pair is separated into the two QDs, as depicted in Fig. 1b. The non-dissipative Josephson current that flows in the presented system is captured in the Josephson energy of the junction (E_J), which indicates the potential energy stored and is proportional to the critical current ($E_J \propto I_c$). E_J can be written as a sum of three components.

$$E_J = E_{J1}(\epsilon_{d1}) + E_{J2}(\epsilon_{d2}) + E_{J12}(\epsilon_{d1}, \epsilon_{d2}), \quad (1)$$

where $E_{J1}(\epsilon_{d1})$ and $E_{J2}(\epsilon_{d2})$ are the contributions to E_J for the local tunnelling of a Cooper pair through QD1 and QD2, respectively, and $E_{J12}(\epsilon_{d1}, \epsilon_{d2})$ is the contribution for non-local transport processes in which a Cooper pair is split between the two QDs and then recombined as shown in Fig. 1b. Note that E_{J12} is a function of the energy levels of both QDs. The local processes are suppressed by the on-site charging energy of each QD (U_1 and U_2), which prevents the tunnelling of two electrons. The non-local process is unaffected by the on-site charging energy but its probability decreases with the separation of the contacts to the two QDs (the distance over which the Cooper pair must be separated inside the contact).

The proposed scheme to detect the contribution to the Josephson current arising from the non-local processes is to tune one QD to be OFF resonance such that only the other QD contributes to the transport and use measurements under these conditions as a background or reference for comparison with transport when both QDs are ON or near resonance. One complication of this treatment is that the sign of each component of the Josephson energy maybe positive or negative depending on the specifics of the QD occupation and the number and parity of the orbital states involved in the transport²². The measurement of the switching current of the device only provides an absolute measurement of the Josephson current. By measuring the

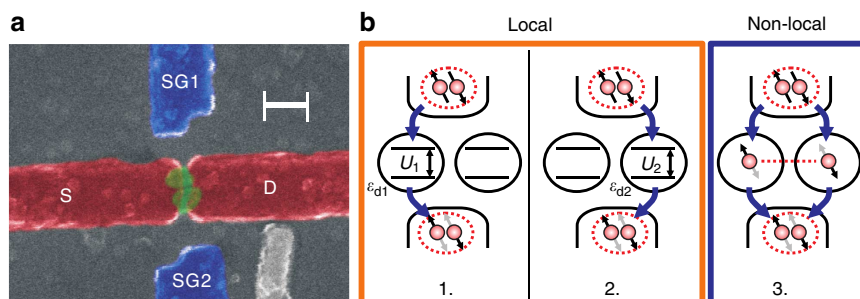


Figure 1 | Sample image and schematic. (a) False colour scanning electron microscope image of the device with side-gates (SG) and source (S) and drain (D) electrodes indicated. Scale bar, 150 nm. (b) Schematic of the three lowest order (fourth order) Cooper pair tunnelling processes. In processes (1) and (2), the Cooper pair tunnels through a single QD. In process (3), the Cooper pair is split through both QDs and a non-local entangled state (EPR state) is achieved. In each process, the specifics of the tunnelling and the parity of the QD occupation may result in reversal of the spin order of the Cooper pair giving a negative contribution to the Josephson energy of the junction.

supercurrent, we detect only processes that result in the phase coherent tunnelling of a pair of electrons in the singlet state. In practice, it is possible for the two QDs to be occupied by electrons in the triplet state, which cannot contribute to the supercurrent and will therefore not be measured.

Normal state characterization. Before examining the superconducting transport, we discuss transport in the normal state when a magnetic field (B) is applied perpendicular to the sample surface. In this configuration, the critical magnetic field of the aluminium leads is $B_c \sim 110$ mT. An example of the normal state charging stability diagram is presented in Fig. 2a for $B = 160$ mT. Despite the physical proximity of the two QDs, we observe negligible interdot tunnel capacitive coupling, which maybe expected to vary with the specific charge states but is evaluated as being $< 30 \mu\text{eV}$ in the regions that we have studied and is therefore smaller than the superconducting energy gap (see Supplementary Fig. 1 and Supplementary Note 1). We conclude therefore that the nanogap electrodes very effectively screen the two QDs. The side-gate electrodes are able to independently tune the occupation of the two QDs with only a small effect on QD1 from $V_{\text{sg}2}$ and vice versa. Both QDs are operated in the many electron regime (a few tens of electrons) for which the energy level spacing and charging energy vary with orbital state²³. Using stability plots measured under various conditions, we extract typical ranges for the charging energies of $U_1 \sim 2 - 4$ meV and $U_2 \sim 2 - 5$ meV. Similarly, typical energy level spacings are evaluated in the ranges $\delta\epsilon_{\text{d}1} > 3 - 4$ meV and $\delta\epsilon_{\text{d}2} \sim 1 - 4$ meV. By tuning the charge state using the backgate, we are able to realize a wide range of different QD-lead tunnel coupling (Γ), evaluated in the normal state from the width of Coulomb peaks²⁴, in the range $\Gamma = 0.1 - 1.5$ meV. Typically, we find that $\delta\epsilon_{\text{d}1}, U \gtrsim \Gamma > \Delta$ such that the device is in the intermediate coupling regime²⁵. The large energy level spacing and charging energy compared with the Aluminium superconducting energy gap ($\Delta \sim 130 \mu\text{eV}$, see Supplementary Fig. 2 and Supplementary Note 2) indicates that a single-level picture is a reasonable approximation for the system. No signature of interdot tunnel coupling is seen for any of the charge states we have studied and so a lower bound for the

possible interdot coupling can be estimated from the lowest dot-lead tunnel couplings measured indicating $\gamma_{\text{interdot}} \ll 0.1$ meV and consequently $\gamma_{\text{interdot}} \ll \Delta$. The charging energies and other parameters may alter slightly when the side-gates are swept^{23,24,26}; however, these changes are typically smooth and small for this sample over the gate ranges we are considering. At high magnetic fields, we observe clear Aharonov–Bohm oscillations, which are consistent with the small dimensions of the junction (Supplementary Fig. 3 and Supplementary Note 3) and indicate that coherent transport through the parallel QDs is possible despite the short coherence length in the metal contacts. We also observe an anomalous conductance feature when both QDs are tuned ON resonance in the normal state, which is discussed in Supplementary Figs 4–8 and Supplementary Note 4.

Superconducting transport. We now consider the measurement of the junction critical current and anomalous transport features, which we attribute to the non-local Cooper pair tunnelling in the double QD Josephson junction. Typical $V(I)$ traces at $B = 0$ T are shown in Fig. 2b. For the ranges of side-gate bias and backgate bias studied in this report, the junction is predominately underdamped indicating that the dissipation in the circuit is weak compared with the phase changes (fluctuations) across the junction. $V(I)$ traces display characteristic hysteretic switching between Josephson current and normal dissipative current branches. The transport is characterized by a switching current (I_{sw}), which is taken as proportional to the junction critical current and a retrapping current (I_r). Recent studies indicate that the hysteresis likely arises from the heating of the junction in the normal state rather than effects related to the dynamics of the junction²⁷. The signature of the non-local processes has been studied in several different transport regions with different relative couplings of the individual QDs (see also Supplementary Fig. 9 and Supplementary Note 5). Where indicated, the even and odd electron occupation of each QD has been confirmed either by observation of the Zeeman splitting of Coulomb peaks or features in the superconducting transport associated with the odd electron occupation such as asymmetric supercurrent when the gate is swept across a Coulomb peak²⁴ (see Supplementary Figs 10 and

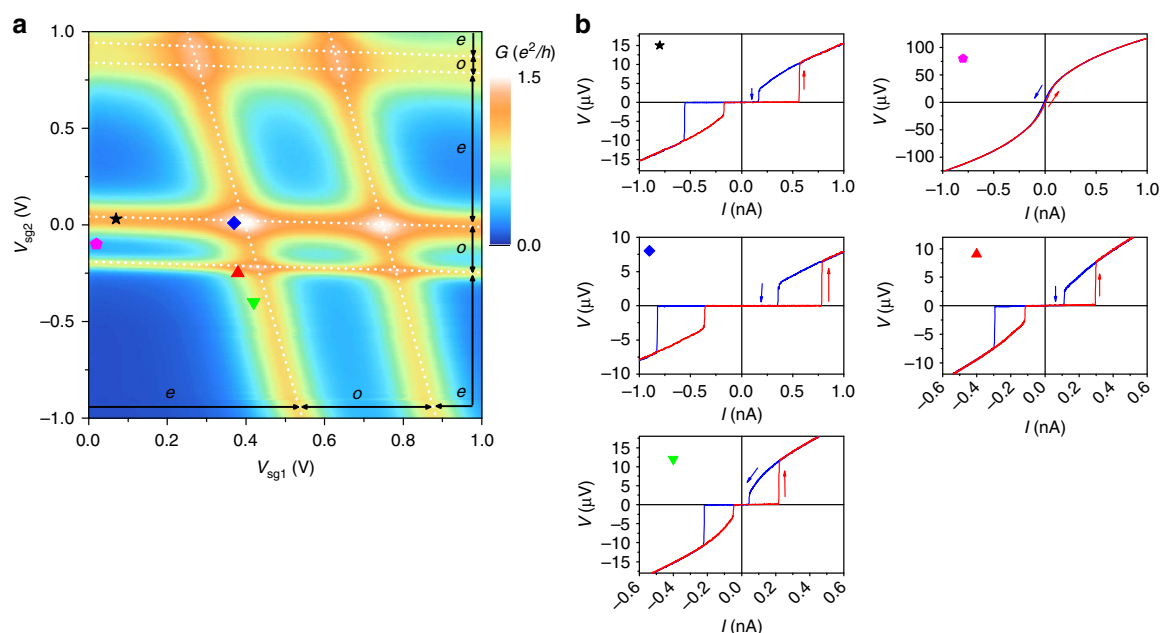


Figure 2 | Device characterization. (a) Plot of the differential conductance (dI/dV_{sd}) as a function of $V_{\text{sg}1}$ and $V_{\text{sg}2}$ with $V_{\text{sd}} = 0$ V, $B = 160$ mT applied out-of-plane and $V_{\text{bg}} = 0$ V. (b) Example $V(I)$ traces measured at the the points indicated in a. Arrows indicate the current sweep direction.

11 and Supplementary Note 6). In the remaining figures (Figs 3–5), we study the measured I_{sw} in the superconducting state as a function of V_{sg1} and V_{sg2} . The measured I_{sw} is extracted at each data point from $V(I)$ plots as shown in Fig. 2b. The signatures of the non-local or split Copper pair tunnelling are discussed in the section which follows.

Discussion

Consider the measurements presented in Fig. 3 collected for a region of the gate parameter space in which QD2 is relatively strongly coupled compared with QD1. To allow study of the non-local current, we extract traces along lines A–E, which are parallel with the Coulomb charging peaks for QD2, and use these to compare I_{sw} with both QDs ON resonance (trace A) to I_{sw} with only one QD ON resonance (traces B and C). Initially, we consider the Josephson current when both QDs are tuned to be far OFF resonance. When one QD is tuned to be OFF resonance, the Josephson current arising from local Cooper pair tunnelling through that QD is negligible as a result of the large U . The non-local processes are most efficient when both QDs are near resonance so by tuning both QD far from resonance the non-local contribution can be minimized or even zero. Indeed, we find in our device that with both QDs in the Coulomb blockade we can detect no supercurrent. Next we consider traces B and C in Fig. 3c, which are taken for the condition that QD2 is far OFF resonance. Here when QD1 is also away from resonance (in the

Coulomb blockade), for example, point ③, we observe that $I_{sw} = 0$ indicating that $E_{J1}, E_{J2}, E_{J12} \sim 0$ as previously discussed. Similarly at point ④, where QD1 has an odd electron occupation but is OFF resonance, we observe that $I_{sw} = 0$. When V_{sg1} is tuned QD1 is brought into or ON resonance at points ① and ②. At these points, a peak in I_{sw} is observed as the local tunnelling processes allow a supercurrent to flow. As QD2 is OFF resonance $E_{J2} \sim 0$, and so the supercurrent is given by $E_J = E_{J1} + E_{J12}$. We may naively assume that E_{J12} is negligible such that the measured I_{sw} largely reflects the local transport through QD1.

We now consider the case where QD2 is ON resonance as shown in trace A. Here tuning V_{sg1} shifts QD1 ON and OFF resonance allowing us to observe the effects on the supercurrent. When QD1 is brought ON resonance peaks in I_{sw} are observed that arise from all available transport processes both local and non-local. Furthermore, a reduction in I_{sw} is seen when QD1 has an odd electron occupation in the Coulomb blockade, a condition for which in traces B and C no supercurrent was detected. We take the level of I_{sw} at point ③ of trace A (selected as QD1 is OFF resonance with even occupation) as a reference, indicated by the colour fill in Fig. 3c, to better visualize the anomalous features. We stress, however, that at point ③, we cannot rule out a finite non-local contribution E_{J12} and so in our analysis we are unable to evaluate absolute contributions from the non-local processes (or confidently select a background level for the local transport through QD2). We assume that the influence of local transport through QD1, $E_{J1}(e_{d1})$, is captured in traces B and C where QD2

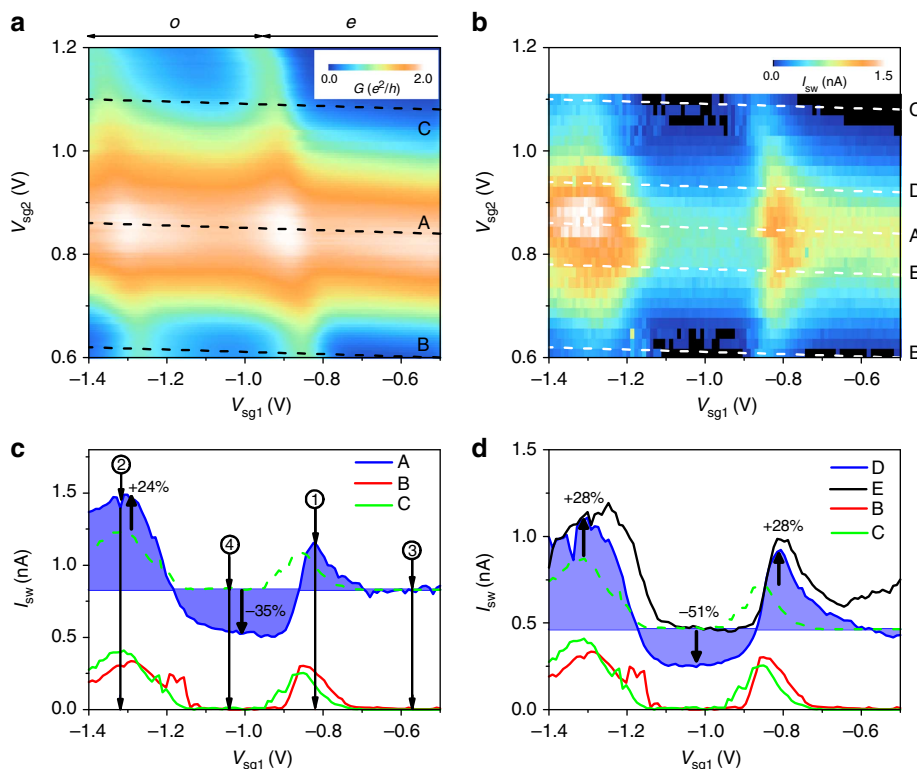


Figure 3 | Superconducting state transport measurement A. (a) dI/dV_{sd} plotted as a function of V_{sg1} and V_{sg2} with $V_{bg} = 0$ V and $B = 160$ mT applied out-of-plane. Labels o and e indicate even and odd electron occupation respectively. (b) I_{sw} plotted as a function of V_{sg1} and V_{sg2} with $V_{bg} = 0$ V and $B = 0$ T. (c) I_{sw} extracted along lines A, B and C in plot (b). The background indicated for trace A is taken as the value of I_{sw} measured at point ③ ($V_{sg1} = -0.57$ V) where QD1 is OFF resonance. Points ① ($V_{sg1} = -1.32$ V), ② ($V_{sg1} = -0.824$ V) and ④ ($V_{sg1} = -1.04$ V) are discussed in the main text. The dashed line indicates trace C offset by the current at point ③ of trace A. Arrows and percentages indicate the approximate increase (decrease) in I_{sw} evaluated by the deviation of trace A from the dashed reference line. (d) I_{sw} extracted along lines B, C, D and E in plot (b). The dashed line indicates trace C offset by a background I_{sw} taken at a point where QD1 is OFF resonance in trace D. Arrows and percentages indicate the relative enhancement and suppression of I_{sw} evaluated by the deviation of trace D from the dashed reference line. Lines D and E are taken to be near resonance with QD2 and show a larger relative enhancement compared with the both QD ON resonance condition (line A in c).

is OFF resonance. As we observe in traces B and C that $I_{sw} = 0$, and therefore $E_{j1} \sim 0$, in the QD1 Coulomb blockade we can attribute features in this region when QD2 is ON resonance as arising only from $E_j = E_{j2} + E_{j12}$. As there is a clear variation of I_{sw} when the occupation parity of QD1 is altered, we can write that at point ④ of trace A the Josephson energy is given by $E_j = E_{j2} + E_{j12}^{QD1\text{odd}}$ and at point ③ it is given by $E_j = E_{j2} + E_{j12}^{QD1\text{even}}$. At point ④ of trace A, we observe a $\sim 35\%$ reduction of I_{sw} compared with reference point ③. We are able to subtract out the local transport processes through QD2 by finding the difference between I_{sw} at points ③ and ④ resulting in $E_{j12}^{QD1\text{odd}} - E_{j12}^{QD1\text{even}}$, which gives an order estimate of a contribution of the non-local process to supercurrent of $\Delta I_{sw} \sim 0.3$ nA. As previously mentioned, it is possible that the non-local process results in a negative contribution to the Josephson energy either due to occupation parity or orbital parity. In Supplementary Figs 12–16 and Supplementary Note 7, we consider the possibility that the tuning of one QD ON/OFF resonance alters the dissipation in the circuit causing a change in the measured I_{sw} . By measuring the hysteresis in the $V(I)$ traces we investigate changes due to the variation of the local electromagnetic environment. We observe that while the hysteresis is altered by tuning the device gates the features are not correlated with the enhanced and suppressed I_{sw} identified as a signature of the non-local transport. We still however cannot exclude a small effect due to changes in the dissipative environment of the junction due to one QD acting as a tunable shunt for the second QD.

We can also consider I_{sw} at points ① and ② where both QDs are ON resonance. Through comparison with traces B and C with trace A, we observe a $\sim 24\%$ increase in I_{sw} at point ②. At point ①, however, I_{sw} is approximately equal to the sum of OFF resonance I_{sw} for each QD. While we cannot extract the non-local contribution in the reference data at these points, we do not expect the local contributions to alter indicating that the enhancement of I_{sw} originates from a large increase in E_{j12} with both QDs ON resonance at point ②. We also consider the case of QD2 near resonance in Fig. 3d and observe that the relative contribution from non-local processes is increased as the local transport through QD2 is reduced when tuned away from resonance.

To show that the features are reproducible, we consider another region of the gate parameter space, presented in Fig. 4a, which is measured on a different cooldown of the same device. In this case, a wider gate range is studied in which QD1 exhibits two Coulomb peaks with a relatively stronger coupling than QD2,

giving higher local supercurrents than QD2. As in our previous analysis, we extract traces A–C taken with QD1 ON (trace A and B) and OFF (trace C) resonance, Fig. 4b. In trace C with QD1 OFF resonance, we again only observe finite supercurrent under conditions for which QD2 is brought ON or near resonance. In traces A and B, we again plot data with a colour fill to a background selected as the even occupation Coulomb blockade of QD2 taken at point ①. We observe that for some regions with odd electron occupation I_{sw} is reduced indicating the influence of the non-local transport processes as the local transport through QD1 is not influenced by the parity of QD2. We also observe the enhancement of I_{sw} when both QDs are ON or near resonance but more clearly than in Fig. 3c. The enhanced and reduced supercurrent again provide clear signature of the non-local Cooper pair tunnelling process. The parity effect of the OFF resonance QD on the non-local Cooper pair tunnelling as observed in Figs 3 and 4 appear pronounced when the OFF resonance QD is weakly coupled compared with the other ON resonance QD. For both QDs, approximately similarly coupled to the leads we also observe the parity effect albeit less pronounced. Finally, we consider the region in Fig. 5 that shows I_{sw} evaluated

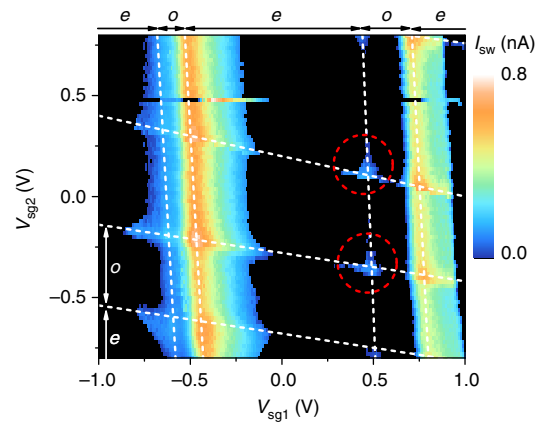


Figure 5 | Superconducting state transport measurement C. I_{sw} as a function of V_{sg1} and V_{sg2} with $V_{bg} = 1.6$ V and $B = 0$ T. Dashed lines indicate the positions of Coulomb charging peaks. Labels o and e indicate regions of odd and even electron occupation where known. Circled regions indicate the points discussed in the text at which QD1 and QD2 are both ON resonance and the majority of supercurrent arises from the non-local tunnelling.

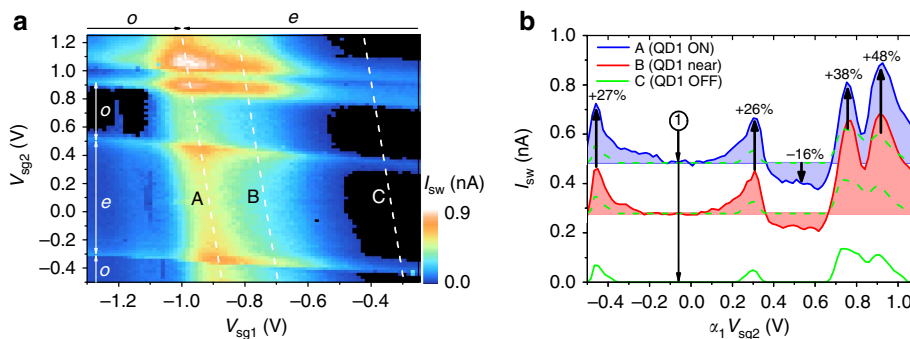


Figure 4 | Superconducting state transport measurement B. (a) I_{sw} as a function of V_{sg1} and V_{sg2} at $V_{bg} = 0$ V and $B = 0$ T. Dashed lines indicate the traces A, B and C plotted in b. Labels e and o indicate even and odd electron occupation, respectively. (b) I_{sw} traces as a function of $\alpha_2(V_{sg1})V_{sg2}$ extracted along lines indicated in plot a. The variable α_2 corrects for the influence of V_{sg1} on QD2 for easier comparison of the traces. The backgrounds for the colour fill for traces A and B are taken as I_{sw} measured at point ① ($\alpha_2 V_{sg2} = -0.059$) where I_{sw} with QD2 OFF resonance is zero (seen in trace C). The dashed lines indicate trace C offset (again by the I_{sw} and point ①) for comparison with trace A and trace B. Arrows and percentages indicate the approximate increase (decrease) in I_{sw} when QD1 and QD2 are ON or near resonance (QD1 ON/near resonance and QD2 with odd occupation).

for a wide range of side-gate voltages showing a variation in switching current for different Coulomb peaks. As previously discussed, the coincidence of the resonance conditions with both QDs results in an enhanced supercurrent for the junction. The effect here is particularly prominent for the two circled coincident resonance conditions as for the relevant QD1 and QD2 Coulomb peaks for these crossings we observe no supercurrent away from the crossing point. This indicates that the local transport of these states is completely suppressed. The peak observed in the supercurrent when both QDs are ON resonance can then be considered to arise from only non-local processes in this case.

In summary, we fabricate a single Josephson junction containing two InAs self-assembled QDs in parallel and close proximity such that a Josephson current may flow by splitting of single Cooper pairs between the two QDs. This non-local transport path that indicates the spatially split entangled pair is identified from the comparison of the Josephson current measured when the QDs are tuned ON/OFF resonance using local gates. Experimentally, we have observed similar signatures in various regions and devices in a wide range of asymmetry in the tunnel couplings of QD1 and QD2. Further studies of the non-local spin entangled state maybe achieved by including an additional pilot Josephson junction or using superconducting material with high critical magnetic fields to allow manipulation of the superconducting phase difference across the double dot Josephson junction^{19,21}.

Methods

Fabrication details. The InAs self-assembled QDs were grown by molecular beam epitaxy on a (100)-oriented GaAs substrate. The growth layers on the substrate consist of a 200-nm thick degenerately Si-doped layer, used as the backgate, followed by a 100-nm thick $Al_{0.3}Ga_{0.7}As$ barrier layer and a 200-nm thick undoped GaAs buffer layer. The InAs QDs were formed through the Stranski-Krastanov growth mode from a wetting layer of ~ 4 monolayers of InAs which results in a mixed phase of large and small QDs. To accurately contact two QDs in close proximity, we first deposit arrays of Ti/Au alignment markers using electron beam lithography and evaporation. We then use atomic force microscopy to identify suitable pairs of QDs. Finally the targetted pairs were contacted and side-gates were added using a single electron beam lithography step. To achieve transparent superconducting contacts, the QDs are exposed to a weak Argon plasma *in situ* within the processing chamber before deposition of (3/150 nm) Ti/Al contacts by electron beam evaporation.

Measurement details. Measurements are performed in a dilution refrigerator with a 30-mK base temperature and equipped with a superconducting magnet. The measurement lines were filtered with a series of room temperature and cold filters. These include commercial pi-filters (minicircuits BLP-1.9+) at room temperature, and custom-made copper powder and RC filters mounted at the mixing chamber stage of the fridge. Following the filters, the sample itself was mounted in an rf-tight copper enclosure.

References

1. Einstein, A., Podolsky, B. & Rosen, N. Can quantum-mechanical description of physical reality be considered complete? *Phys. Rev.* **47**, 777–780 (1935).
2. Aspect, A., Grangier, P. & Roger, G. Experimental realization of Einstein-Podolsky-Rosen-Bohm gedankenexperiment: a new violation of bell's inequalities. *Phys. Rev. Lett.* **49**, 91–94 (1982).
3. Bennet, C. & DiVincenzo, D. Quantum information and computation. *Nature* **404**, 247–255 (2000).
4. Ursin, R. *et al.* Entanglement-based quantum communication over 144 km. *Nat. Phys.* **3**, 481–486 (2007).
5. Lesovik, G. B., Martin, T. & Blatter, G. Electronic entanglement in the vicinity of a superconductor. *Eur. Phys. J. B* **24**, 287–290 (2001).
6. Recher, P., Sukhorukov, E. V. & Loss, D. Andreev tunneling, coulomb blockade, and resonant transport of nonlocal spin-entangled electrons. *Phys. Rev. B* **63**, 165314–165324 (2001).
7. Recher, P. & Loss, D. Superconductor coupled to two luttinger liquids as an entangler for electron spins. *Phys. Rev. B* **65**, 165327–165340 (2002).
8. Bena, C., Vishveshwara, S., Balents, L. & Fisher, M. Quantum entanglement in carbon nanotubes. *Phys. Rev. Lett.* **89**, 037901–037904 (2002).
9. Chitchekatchev, N., Blatter, G., Lesovik, G. & Martin, T. Bell inequalities and entanglement in solid-state devices. *Phys. Rev. B* **66**, 161320–161323 (2002).

10. Recher, P. & Loss, D. Dynamical coulomb blockade and spin-entangled electrons. *Phys. Rev. Lett.* **91**, 267003–267006 (2003).
11. Bouchiat, V. *et al.* Single-walled carbon nanotube-superconductor entangler: noise correlation and einstein-podolsky-rosen states. *Nanotechnology* **14**, 77 (2003).
12. Falci, G., Feinberg, D. & Hekking, F. W. J. Correlated tunneling into a superconductor in a multiprobe hybrid structure. *Europhys. Lett.* **54**, 255–261 (2001).
13. Oh, S. & Kim, J. Entanglement of electron spins in superconductors. *Phys. Rev. B* **71**, 144523–144526 (2005).
14. Herrmann, L. *et al.* Carbon nanotubes as cooper-pair beam splitters. *Phys. Rev. Lett.* **104**, 026801–026804 (2010).
15. Schindele, J., Baumgartner, A. & Schönenberger, C. Near-unity cooper pair splitting efficiency. *Phys. Rev. Lett.* **109**, 157002–157006 (2012).
16. Hofstetter, L., Csonka, S., Nygård, J. & Schönenberger, C. Cooper pair splitter realized in a two-quantum-dot Y-junction. *Nature* **461**, 960–963 (2009).
17. Das, A. *et al.* High-efficiency cooper pair splitting demonstrated by two-particle conductance resonance and positive noise cross-correlation. *Nat. Commun.* **3**, 1165 (2012).
18. Leijnse, M. & Flensberg, K. Coupling spin qubits via superconductors. *Phys. Rev. Lett.* **111**, 060501–060505 (2013).
19. Choi, M.-S., Bruder, C. & Loss, D. Spin-dependent josephson current through double quantum dots and measurement of entangled electron states. *Phys. Rev. B* **62**, 13569–13572 (2000).
20. Pan, H. & Lin, T. Control of the supercurrent through a parallel-coupled double quantum dot system. *Phys. Rev. B* **74**, 235312–235319 (2006).
21. Wang, Z. & Hu, X. Interference and switching of Josephson current carried by non-local spin-entangled electrons in a squid-like system with quantum dots. *Phys. Rev. Lett.* **106**, 037002–037005 (2011).
22. van Dam, J., Nazarov, Y., Bakkers, E., de Franceschi, S. & Kouwenhoven, L. Supercurrent reversal in quantum dots. *Nature* **442**, 667–670 (2006).
23. Kanai, Y. *et al.* Electrically tuned spinorbit interaction in an inas self-assembled quantum dot. *Nat. Nanotechnol.* **6**, 511–516 (2011).
24. Kanai, Y. *et al.* Electrical control of kondo effect and superconducting transport in a side-gated InAs quantum dot josephson junction. *Phys. Rev. B* **82**, 054512–054519 (2010).
25. Franceschi, S. D., Kouwenhoven, L., Schönenberger, C. & Wernsdorfer, W. Hybrid superconductor/quantum dot devices. *Nat. Nanotechnol.* **5**, 703–711 (2010).
26. Deacon, R. *et al.* Electrically tuned g-tensor in an InAs self-assembled inas quantum dot. *Phys. Rev. B* **84**, 041302–041305(R) (2011).
27. Courtois, H., Meschke, M., Peltonen, J. T. & Pekola, J. P. Origin of hysteresis in a proximity josephson junction. *Phys. Rev. Lett.* **101**, 067002–067005 (2008).

Acknowledgements

We acknowledge fruitful discussions with Rui Sakano. Part of this work was supported by Grant-in-Aid Research A from No. 25246004 and 25246005 and Innovative areas (No. 21102003) and (No. 26103004) MEXT, JST Strategic International Cooperative Program (DFG-JST), FIRST program, ImPACT Program of Council for Science, Technology and Innovation (Cabinet Office, Government of Japan) and MEXT Project for Developing Innovation Systems.

Author contributions

R.S.D. fabricated the devices, performed the measurements, analysed the results and wrote the manuscript. A.O., J.S., S.B. and Y.K. contributed to the data acquisition, data interpretation and device design. K.S. and K.H. grew the uncapped InAs QDs. S.T. contributed to the interpretation of results and supervised the work. All authors contributed to the discussions and writing of the manuscript.

Additional information

Supplementary Information accompanies this paper at <http://www.nature.com/naturecommunications>

Competing financial interests: The authors declare no competing financial interests.

Reprints and permission information is available online at <http://npg.nature.com/reprintsandpermissions/>

How to cite this article: Deacon, R. S. *et al.* Cooper pair splitting in parallel quantum dot Josephson junctions. *Nat. Commun.* 6:7446 doi: 10.1038/ncomms8446 (2015).



This work is licensed under a Creative Commons Attribution 4.0 International License. The images or other third party material in this article are included in the article's Creative Commons license, unless indicated otherwise in the credit line; if the material is not included under the Creative Commons license, users will need to obtain permission from the license holder to reproduce the material. To view a copy of this license, visit <http://creativecommons.org/licenses/by/4.0/>